This article has been accepted for publication in a future issue of this journal, but has not been fully edited. Content may change prior to final publication. Citation information: DOI 10.1109/TAP.2018.2851367, IEEE Transactions on Antennas and Propagation

Characterization of Wideband Antennas for Point-to-Point Communications

Mohammed A. Almoteriy, *Student Member, IEEE*, Mohamed I. Sobhy, *Life Member, IEEE*, and John C. Batchelor, *Senior Member, IEEE*

***Abstract*—Antenna frequency response can be characterized in terms of effective aperture and gain. Antennas can also be characterized as a two-port network to ascertain the antenna transfer function (S_{21}). This characterization is important in point-to-point (P2P) communication, as the frequency response can vary due to changes in the radiation pattern in the physical channel. This paper presents a process to investigate the frequency response of a wideband antenna in order to identify the best orientation of the antenna for P2P communication. The process predicts the antenna's effective aperture and gain for each orientation. An equivalent circuit for the wideband antenna is also derived to obtain the total radiated power. The frequency-variant radiation pattern is ascertained from the S_{21} phase obtained from the equivalent circuit. For each orientation, the S_{21} phase is analyzed based on the linear, minimum, and all-pass phase components, which enables the derivation of an equivalent circuit. The variation of group delay for each orientation is also obtained and compared. The measurements between two identical antennas at the two orientations with a free-space channel were then modeled for simulation in a digital system. This simulation predicts the antenna effects for the two orientations used. Finally, this process was validated by using a non-minimum phase monopole ultra-wideband (UWB) antenna.**

***Index Terms*—Ultrawideband antennas, transfer functions, circuit modeling, phase distortion, digital systems.**

I. Introduction

A conventional antenna design procedure starts by designing the antenna for a low reflection coefficient (S_{11}), following which the radiation pattern, antenna gain, effective aperture, and polarization are obtained for certain frequencies of operation. However, these steps do not provide the performance of the antenna with respect to its physical orientation, especially for point-to-point (P2P) communication applications and situations where the direction of the main beam may be a function of frequency. The S_{11} value alone allows the total radiated power to be appreciated but provides no insight into the beam direction or its frequency dependence. It is important to distinguish between the total radiated power and the radiated power in the direction of the physical channel. The conventional procedure to obtain the frequency response in terms of effective aperture and gain requires measurement or simulation of the radiation pattern at a large number of frequencies, which is often impractical.

M. A. Almoteriy, M. I. Sobhy, and J. C. Batchelor are with the School of Engineering and Digital Arts, University of Kent, Canterbury CT2 7NT, U.K. (e-mail: {maa74; m.i.sobhy; j.c.batchelor}@kent.ac.uk)

Ultra-wideband (UWB) antennas have an operating bandwidth from 3.1 to 10.6 GHz [1], where the function is to achieve high data rates without errors. For most UWB antennas in P2P communications, the frequency response of the physical channel between the transmitting and receiving antennas is dependent upon the orientation of the antennas [1]. The physical channel is usually selected based on the direction of the main beam of the fundamental radiation pattern (i.e., the principal axis). Further parameters such as the frequency-variant radiation pattern and current distribution are also required for designing UWB antennas [2]-[5]. Although various techniques have been proposed recently by modifying the geometry of the UWB antenna in order to have a frequency-invariant radiation pattern [2]-[5], the radiation patterns are only represented at certain discrete frequencies, which does not predict the performance or the behavior of the antenna over the entire operating bandwidth.

Representing an antenna as a two-port equivalent circuit would help the designer relate the frequency response to the antenna's physical structure. The antenna equivalent circuit can be derived from the amplitude and phase of S_{11}, and researchers have expressed interest in the development of an accurate equivalent lumped circuit for UWB antennas. Studies to date have primarily considered the amplitude response of S_{11} and ignored the phase [6]-[8], which does not provide an accurate complex transfer function (S_{21}) of the antenna. Including the phase as well as the amplitude of S_{11} preserves information about antenna parameters and properties such as input impedance (Z_{11}) and S_{21} as well as the behavior of the antenna as a resonant structure and the antenna's frequency-variant radiation pattern.

Antennas can be categorized into minimum and non-minimum phase [9]-[11]. The phase of S_{21} is related to the path of energy transmission across its equivalent circuit [12]. Therefore, the minimum phase of S_{21} can occur only if one path exists through the circuit. For instance, a ladder network has minimum phase. Research shows that not all antennas provide a minimum phase. Well-known minimum-phase examples include the horn and Vivaldi designs [9]-[11], both of which are minimum phase only at their principal axes [12], [13]. To the best of the authors' knowledge, no comprehensive studies have yet been conducted to determine the transmission phase response in the performance of non-minimum phase antennas.

In a wideband communication system, the variation of group delay (GD) is critical, in that a large variation can distort the signal, and the GD depends on the phase of S_{21} [14]. Modulated symbols emitted from a non-minimum phase antenna on its principal axis can be distorted because different frequencies

This article has been accepted for publication in a future issue of this journal, but has not been fully edited. Content may change prior to final publication. Citation information: DOI 10.1109/TAP.2018.2851367, IEEE Transactions on Antennas and Propagation

manifest different delays through the system. This distortion further increases the symbol scattering and leads to performance degradation. To avoid signal distortion, the GD over the frequency range should be constant. Therefore, designing an antenna to be minimum phase can mitigate the symbol scattering and also minimize the error vector magnitude (EVM) and bit error rate (BER).

Modeling the antenna as a system allows for antenna simulation in an end-to-end wireless link. Antenna models can be derived as a finite impulse response (FIR) to confirm the compatibility of the antenna with digital communication system simulation [15] and by measuring the full four-set of *S*-parameters using two identical antennas, which increases the antenna modeling accuracy. A previous study has found that some antenna behavior distorts the signal at certain frequencies in the operating range [15], although the effects of antennas at different orientations also needs to be analyzed with respect to the symbol scatter that occurs due to the radiation pattern.

In Section II, the Friis equation is modified in terms of total radiated power and radiated power in a certain direction. The effective aperture and gain are then derived for identical antennas with respect to the frequency axis. Section III presents the design and the electromagnetic (EM) simulation of a non-minimum phase monopole UWB antenna. In Section IV, an equivalent circuit is derived to obtain the S_{21} from the radiation resistance, and to study the antenna behavior. Section V analyzes the amplitude and phase of the S_{21} obtained from the port-to-port transmission using CST, the equivalent circuit, and the measurements at two specific orientations in order to select the best antenna orientation. The variation of GD for each orientation is then calculated and compared. Finally, the two identical antennas with free-space channel are modeled and simulated in a digital communication system to investigate the effect of the antenna in the two orientations.

II. Mathematical Formulation

The performance of the antenna in the free-space far-field region can be described by the Friis equation in terms of effective aperture [16]:

$$P_r = P_t A_t A_r \frac{1}{\lambda^2 R^2} \tag{1}$$

where P_t and P_r are the total transmitted and received power respectively, A_t and A_r are the effective apertures in the direction of the link for the transmitting and receiving antennas respectively, λ is wavelength, and R is the path length of the physical channel.

The effective aperture is given by [16]:

$$A_e = \frac{\lambda^2}{4\pi} G \tag{2}$$

where G is the gain of the antenna.

In terms of the port-to-port S_{21} between the transmitting and receiving antennas, the frequency response of the S_{21} depends on orientations of both antennas. As a result, there are two different transfer scattering parameters, S_{21}^a and S_{21}^b:

(i) $|S_{21}^a|^2$ is the power ratio, representing the total radiated power (radiated power in all directions) for each antenna. S_{21}^a can be calculated from S_{11} for a lossless antenna or from the antenna equivalent circuit as well as antenna simulation. Fig. 1 shows the steps for deriving an equivalent circuit and obtaining S_{21}^a.

(ii) $\left|S_{21}^b\right|^2$ is the power ratio, representing the measured S_{21} between the transmitting and receiving antennas and their physical channels over distance R. S_{21} for each antenna can be calculated from S_{21}^b after de-embedding the free-space channel and dividing by two in dB and radians for the amplitude and phase, respectively. S_{21} of each antenna represents the directional dependency of S_{21}^a.

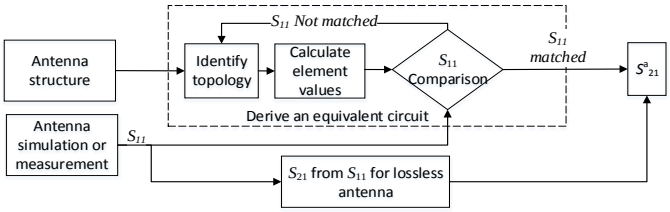

Fig. 1. Method for obtaining S_{21}^a, which represents the total radiated power.

$|S_{21}^a|^2$ and $\left|S_{21}^b\right|^2$ can be represented mathematically as:

$$|S_{21}^a|^2 = \frac{P_t}{P_{av}} \tag{3}$$

$$\left|S_{21}^b\right|^2 = \frac{P_r}{P_{av}} \tag{4}$$

where P_{av} is the power available from the source.

From (3) and (4), (1) can be written in terms of S_{21}^a and S_{21}^b:

$$\left|S_{21}^b\right|^2 = |S_{21}^a|^2 A_t A_r \frac{1}{\lambda^2 R^2} \tag{5}$$

Note that the received power in the direction of the physical channel is a function of frequency, distance, and the effective apertures of the transmitting and receiving antennas. Equation (5) can be applied for non-identical antennas. For identical antennas, the effective aperture and gain can be calculated respectively as:

$$A_e = \lambda R \frac{|S_{21}^b|}{|S_{21}^a|} \tag{6}$$

$$G = \frac{4\pi R}{\lambda} \frac{|S_{21}^b|}{|S_{21}^a|} \tag{7}$$

For a lossless network, the amplitude of the S_{21}^a can be calculated from the amplitude of S_{11} [17]:

$$|S_{21}^a| = \sqrt{1 - |S_{11}|^2} \tag{8}$$

The phase of S_{21} of each antenna can be separated into three components—the minimum, linear, and all-pass phases—as shown in Fig. 2. The linear-phase component represents a constant time delay due to the effective length to the phase center [18], whereas the minimum-phase component represents the amplitude response of the antenna S_{21}. An all-pass

component is an additional phase at certain frequencies in the band. This component arises due to the resonant structure, which affects the frequency-invariant radiation pattern. The all-pass component does not exist in minimum phase antennas (such as horn and Vivaldi antennas) in their principal axes.

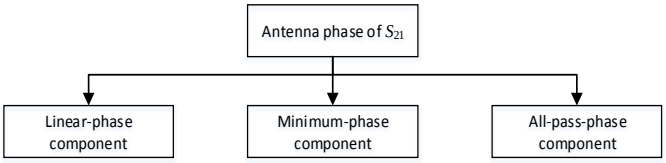

Fig. 2. Phase components of S_{21}.

The Hilbert transform provides the relationship between the real and imaginary part of a function $\mathcal{F}(\mathrm{j}\omega)$, which is analytic in the right-hand side (RHS) of the *s*-plane [19]:

$$\mathcal{F}(\mathrm{j}\omega) = e^{-[\alpha(\omega)+\mathrm{j}\emptyset(\omega)]} \tag{9}$$

where $\alpha(\omega)$ and $\emptyset(\omega)$ are the attenuation and phase of the function, respectively. The attenuation $\alpha(\omega)$ can be calculated by taking logarithms of (9), and the Hilbert transform is used to derive the phase $\emptyset(\omega)$ [19]:

$$\alpha(\omega) = -\ell n|\mathcal{F}(\mathrm{j}\omega)| \tag{10}$$

$$(\omega) = -\frac{1}{\pi}\int_{-\infty}^{\infty}\frac{\alpha(\xi)d\xi}{\omega-\xi} \tag{11}$$

The Hilbert transform extracts a minimum-phase component without any associated linear or all-pass components and can be used to derive the minimum-phase component of the antenna S_{21} obtained from the measurements at different orientations.

III. Antenna Design

A monopole UWB antenna with a coplanar waveguide (CPW) feed [20] was designed and simulated using Computer Simulation Technology (CST) Microwave Studio Suite®. Fig. 3 shows the structure of the antenna, which was etched on a Rogers RT5880 dielectric substrate with a thickness of 1.575 mm and a dielectric constant $\mathcal{E}_r$ of 2.2. S_{11} was obtained from the simulator and compared with measurements from a network analyzer (Fig. 3).

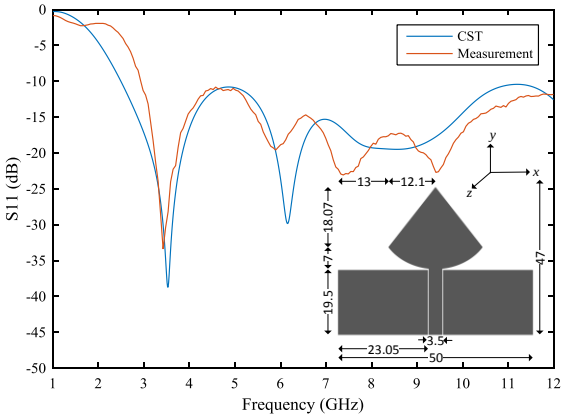

Fig. 3. S_{11} from simulation and measurement, and inset antenna structure (all dimensions in mm).

Figs. 4a and b present the simulated radiation pattern at 4 GHz and 7 GHz, respectively. The direction of the main beam of the radiation pattern at 4 GHz is broadside (principal axis), whereas at 7 GHz the direction of the main beam shifts to azimuth and elevation angles of 90° and 45°, respectively. Note that the broadside gain is very low at 7 GHz, whereas the main beam gain at 7 GHz is slightly higher than at 4 GHz. The current distributions of the antenna were studied at 4 GHz and 7 GHz as shown in Figs. 5a and b respectively. The current intensity increase at the sharp edges of the structure, which causes delay paths in the antenna. It is also clear that the current at 7 GHz is predominantly on the ground plane, which indicates there is a narrow band resonant structure at this frequency.

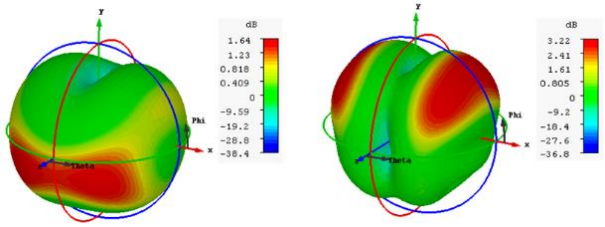

(a) (b)

Fig. 4. Radiation pattern gain at (a) 4 GHz and (b) 7 GHz.

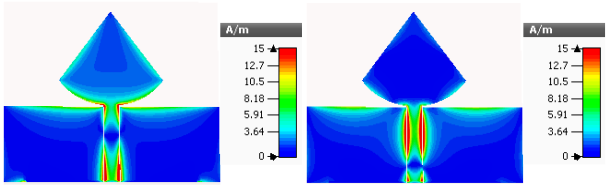

(a) (b)

Fig. 5. Current distribution at (a) 4 GHz and (b) 7 GHz.

The power stimulated in CST was 0.5 W, and the accepted power was obtained from the antenna layout simulation to obtain $|S_{21}^{a}|^2$, which represents the total radiated power. The S_{21}^{b} antenna-to-antenna transmission was also simulated in CST using open boundaries with a 50 cm distance between two identical antennas in the broadside direction. The S_{21}^{b} simulation is compared with the results from the equivalent circuit and the measurements in Section V.

IV. Equivalent Circuit

In antenna two-port equivalent circuits, the second port impedance represents the radiation resistance. The equivalent circuit for the UWB antenna in Fig. 6 was developed by identifying the topology and calculating the element values by applying an iterative optimization process to match the S_{11} measurement. Advanced Design System® (ADS) software was used for the simulation and optimization of the equivalent circuit. Transmission lines were included in the equivalent circuit to represent the distributed elements of the antenna.

As Fig. 7 indicates, the amplitude and phase of S_{11} from the measurement and the ADS equivalent circuit are in agreement. The radiation resistance of the UWB antenna was calculated at approximately 90 Ω. Subsequently, the voltage transfer function was computed from the simulator as the ratio of the voltage across the radiation resistance and the source voltage shown in Fig. 6 in order to obtain S_{21}^{a}, which represents the total radiated power.

This article has been accepted for publication in a future issue of this journal, but has not been fully edited. Content may change prior to final publication. Citation information: DOI 10.1109/TAP.2018.2851367, IEEE Transactions on Antennas and Propagation

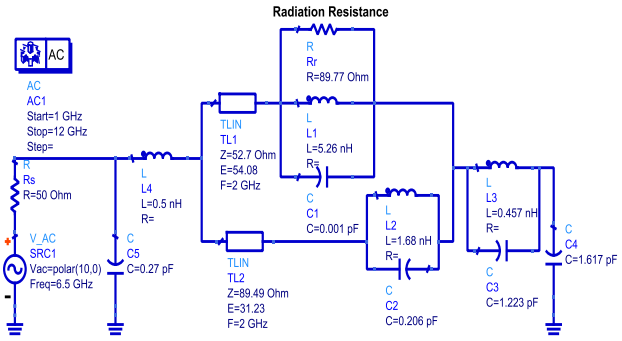

Fig. 6. Equivalent circuit for the UWB antenna.

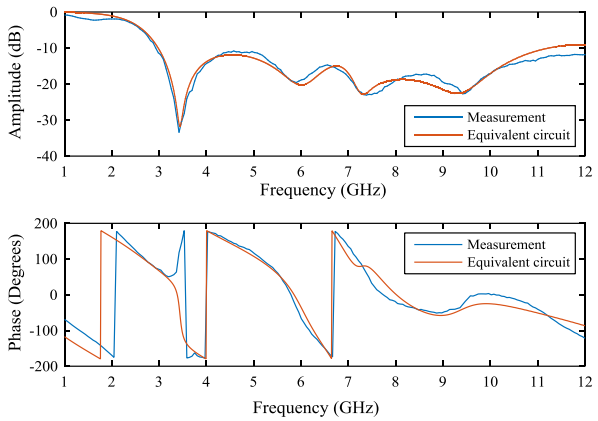

Fig. 7. S_{11} of the UWB antenna from measurement and equivalent circuit.

V. Results and Discussion

Measurements were conducted in an anechoic chamber between two identical UWB antennas with the free-space channel 50 cm apart, using a network analyzer. The reference plane was defined at the end of each cable using the through-open-short-match (TOSM) calibration technique. This was used to measure S_{21}^{b} at two orientations: broadside and a second orientation—where the azimuth and elevation angles were 90° and 45°, respectively—as shown in Fig. 8. Electrical length offset was adjusted to compensate for the connector and the feeding transmission line for each antenna.

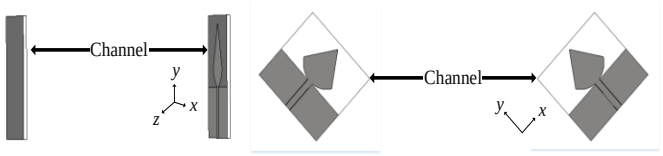

(a) (b)

Fig. 8. Antennas at (a) broadside and (b) second orientation (aligning main beam at 7 GHz).

The measured S_{21}^{b} in the broadside orientation represents the frequency response of the two identical antennas with the free-space channel. The S_{21}^{b} measurement was compared to that obtained from the simulation in CST, as shown in Fig. 9. A similar trend can be seen in the S_{21}^{b} between simulation and measurement. The difference between the plots is a result of inaccurate meshing. Due to the electrically large simulation, domain adaptive mesh refinement is not practical, and so the discretization of the antennas may not be sufficiently accurate to simulate full-wave antenna-to-antenna transmission.

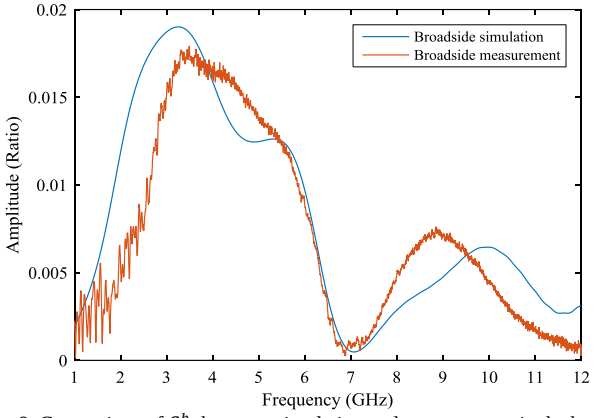

Fig. 9. Comparison of S_{21}^{b} between simulation and measurement in the broadside direction.

The free-space channel was then de-embedded from the measured and simulated S_{21}^{b} based on the distance (50 cm). The amplitude response was obtained based on the Friis transmission equation, and the delay was de-embedded from the phase. This step was done to obtain the amplitude and phase of S_{21} for each antenna at the two orientations. The S_{21} of each antenna represents the directional dependency of S_{21}^{a}. The measurements were made within a frequency range of 1 GHz to 12 GHz. The data was then analyzed and presented from 2 GHz to 11 GHz to avoid band-edge effects.

The amplitude and phase of S_{21}^{a} were also obtained from the equivalent circuit. S_{21}^{a} and S_{21} of the antenna were then compared and analyzed. The variation of GD was obtained for S_{21} of the antenna at the two orientations in order to identify the best orientation for the UWB antenna in P2P communication. Finally, the S_{21}^{b} measurement (two identical antennas with free-space channel) for the two orientations was modeled and simulated in a digital communication system to observe the antenna effects at the two orientations in the digital system, which is discussed in the following sections.

A. S_{21} Amplitude Response

Fig. 10 shows agreement between S_{21}^{a} (which represents the total radiated power) obtained from the antenna simulation, the equivalent circuit, and the calculation from the S_{11} measurement using (8). This agreement confirms the validity of the proposed method to obtain the total radiated power from the antenna equivalent circuit shown in Fig. 1. The agreement also confirms that the antenna is effectively lossless. Fig. 10 also shows agreement in the S_{21} of the antenna between the measurement and simulation in the broadside direction. Fig. 10 also illustrates S_{21} of the antenna obtained from the measurement in the two orientations: broadside and the 7 GHz beam orientation (second orientation). These values represent the radiated power from the transmitting antenna in both directions at the same time versus the frequency. The remaining power is radiated in other directions and eventually dissipates in the sidelobes of the radiation pattern.

This article has been accepted for publication in a future issue of this journal, but has not been fully edited. Content may change prior to final publication. Citation information: DOI 10.1109/TAP.2018.2851367, IEEE Transactions on Antennas and Propagation

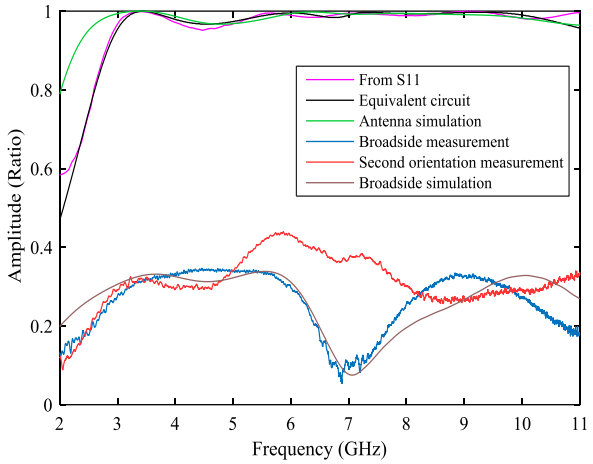

Fig. 10. Comparison of S_{21}^{a} and S_{21} at two orientations.

As expected at 7 GHz, the transmitted power is not steadily radiated in the broadside direction (principal axis). The variation between S_{21}^{a} and S_{21} of the antenna is due to the angular direction of the radiation patterns at each frequency.

Next, (6) and (7) are applied to calculate the effective aperture and gain, which are then compared with the results from the antenna simulation and gain measurements. Fig. 11 illustrates the variation of the effective aperture for broadside and the second orientation. Fig. 12 depicts the difference in the gain of the antenna at the two orientations. The effective aperture at 7 GHz at broadside is very low, and the gain is around -10 dB, whereas the gain in the second orientation generally is more acceptable over the whole frequency band. This scenario indicates that the antenna performance is acceptable for P2P communication when both antennas are positioned in the second orientation.

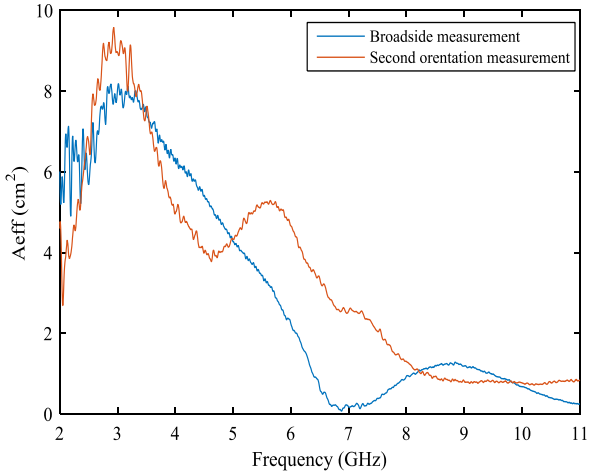

Fig. 11. Effective aperture of the UWB antenna at two orientations.

The gain was also measured in the broadside orientation using a calibrated reference antenna in an anechoic chamber from 4 GHz to 7 GHz. The gain was then compared with that obtained from the proposed process and EM simulation. The measured gain at discrete frequencies are approximately the same as those obtained from the proposed process and the EM simulator, as shown in Table I.

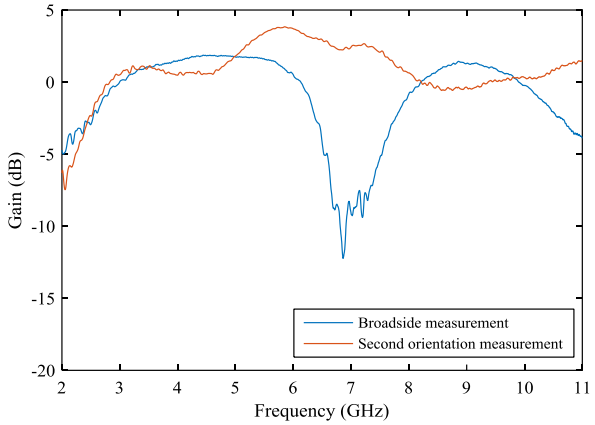

Fig. 12. Gain of the antenna at two orientations from the proposed process.

TABLE I
GAIN IN dB (BROADSIDE ORIENTATION)

Frequency	4 GHz	5 GHz	6 GHz	7 GHz
EM simulation	0.96	0.5	-0.16	-13.9
Gain measurement	0.92	1.63	0.51	-10.1
Proposed process	1.5	1.75	0.5	-9.5

It should also be noted that the current distributions on the antenna are mostly concentrated around the edges, as observed in Figs. 5a and b. This causes a delay in the antenna phase response which is represented by a pair of transmission lines, as shown in the antenna equivalent circuit (Fig. 6). The two different paths in the equivalent circuit indicate that the antenna is non-minimum phase in at least some rotations.

B. S_{21} Phase Components

Fig. 13 illustrates the S_{21} phase of each antenna in the two orientations and the phase of S_{21}^{a} obtained from the antenna equivalent circuit. The phase obtained from the equivalent circuit matches the phase of the broadside S_{21}, because the broadside measurement was in the principal axis direction. As a result, the radiation pattern of the antenna is variant with respect to the frequency due to the non-linearity in the phase of the broadside S_{21} [1], whereas the S_{21} phase in the second orientation is similar to a linear phase.

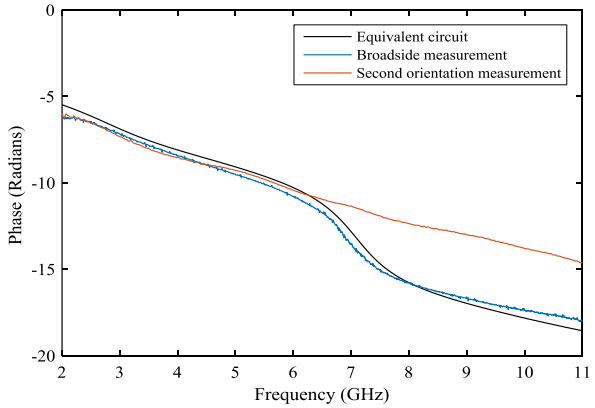

Fig. 13. Phase of S_{21} from circuit and measurements with two orientations.

The second orientation's phase indicates that no additional phase component in S_{21} exists over the frequency band. The S_{21} phase is almost linear because the minimum-phase component is insignificant compared to the linear-phase component.

This article has been accepted for publication in a future issue of this journal, but has not been fully edited. Content may change prior to final publication. Citation information: DOI 10.1109/TAP.2018.2851367, IEEE Transactions on Antennas and Propagation

Recalling that the antenna S_{21} phase consists of three components—minimum, linear, and all-pass phases [9]—the phase of S_{21} with the two orientations is then analyzed from the frequency response to study the antenna's behavior.

The minimum-phase component is computed by applying the Hilbert transform method to the S_{21} amplitude, whereas the linear-phase component is calculated with respect to the antenna's phase center [18]. By identifying the phase center for each orientation, the linear-phase component can be isolated. The all-pass-phase component is obtained after removing the linear and minimum-phase components from the total S_{21} phase obtained from the S_{21}^{b} measurement. The phase components were then characterized for the two orientations as follows.

1) *Broadside* S_{21}: Fig. 14 shows a comparison between the measured phase after removing the linear phase and minimum phase components. Note the differences in phase because of the existing all-pass component within the frequency range 6 GHz to 8 GHz. The large variation of the antenna gain in this direction, as shown in Fig. 12, can only be attributed to the all-pass component of S_{21}, and not to the minimum- or linear-phase components. This variation is also clear from the antenna equivalent circuit because of the existence of more than one path across the equivalent circuit for the energy transferred through the circuit, which again confirms that the antenna is non-minimum phase on the principal axis due to the resonant structure at certain frequencies.

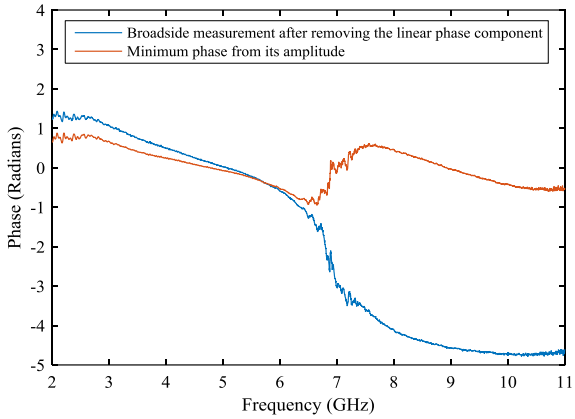

Fig. 14. Minimum phase component and antenna S_{21} phase after removing the linear component in the broadside orientation.

2) *Second Orientation* S_{21}: Fig. 15 illustrates a comparable trend between the phases of S_{21} with the linear-phase component removed as well as S_{21}'s minimum phase. The antenna is nearly minimum phase in this orientation, because the deviation of the calculated gain versus frequency is small, as illustrated in Fig. 12, meaning that the radiated power in this direction continues to radiate over the entire band, with little variation.

This scenario confirms that the antenna is non-minimum phase in the principal axis because of the existing all-pass component. But because there is no all-pass component in the S_{21} phase in the second orientation, the antenna is minimum-phase in this particular angular direction (the second orientation) when the antenna continues to radiate the power over the entire band with little variation, thus indicating that the radiation patterns can provide acceptable gain in this direction over the frequency band.

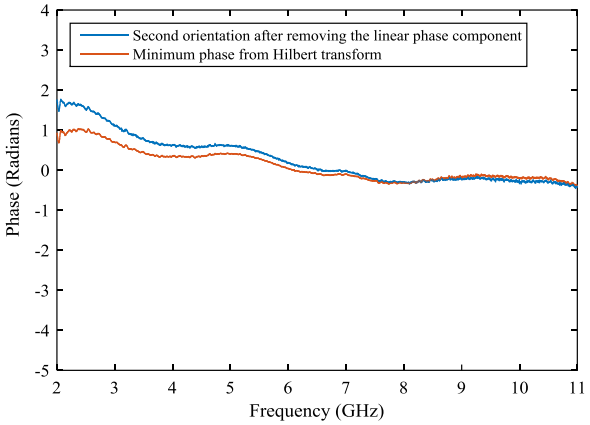

Fig. 15. Minimum phase component and antenna S_{21} phase after removing the linear component in the second orientation.

C. Group Delay

The GD was obtained for the UWB antenna from S_{21} as a function of frequency with the two orientations. Fig. 16 shows the GDs from S_{21} in the broadside and second orientation. The positive large peak within the frequency range 6 GHz to 8 GHz of the GD was obtained from the broadside measurement, which has a negative impact on symbol scattering and the resulting BER at the receiver. This setup also means that the attenuation at the broadside direction was extremely high and that the gain dropped sharply in this range, as shown in Fig. 12. In contrast, the GD obtained from the second orientation S_{21} has little variation over the UWB frequency band, which will introduce a low level of symbol scattering and BER. The second orientation is thus the best choice for P2P communication for this antenna.

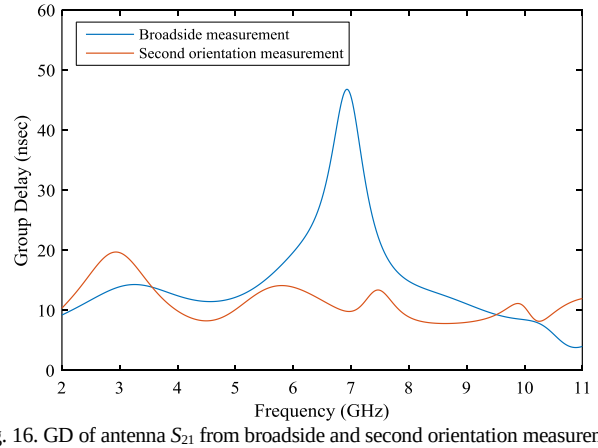

Fig. 16. GD of antenna S_{21} from broadside and second orientation measurements.

D. Digital System Simulation with Two Orientations

FIR filter models were derived for all *S*-parameters obtained from the measurements for each orientation, the S_{21}^{b} having been measured in the anechoic chamber between the two identical antennas with a distance of 50 cm. The complete system models from the measurements at the two orientations were included in a digital communication system, as shown in Fig. 17, which was done to predict the effect of the antenna on the digital system and to calculate the EVM and the BER for characterizing the symbol scatter.

This article has been accepted for publication in a future issue of this journal, but has not been fully edited. Content may change prior to final publication. Citation information: DOI 10.1109/TAP.2018.2851367, IEEE Transactions on Antennas and Propagation

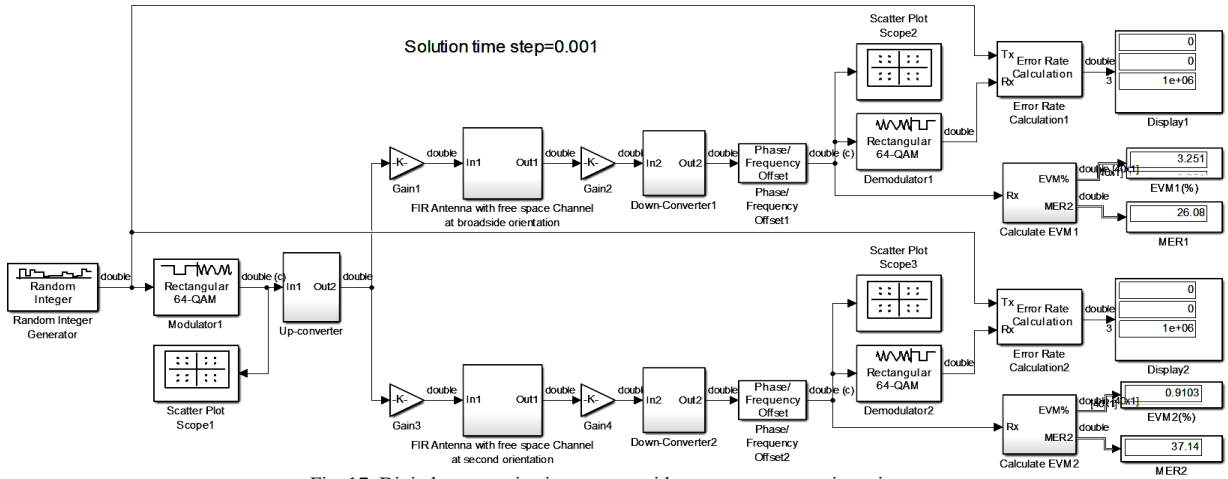

Fig. 17. Digital communication system with antennas at two orientations.

The simulation was done in SIMULINK for 10^6 symbols, with the complete digital communication system having a 64-QAM modulation when a carrier frequency was selected at 3.5 GHz and 6 GHz, respectively. The antenna effects on the 64-QAM modulated signal for the two orientations were examined for each carrier frequency. Figs. 18a and b show constellation diagrams for the broadside and second orientation (respectively) at the receiver with a carrier frequency of 3.5 GHz. The constellation diagrams at 6 GHz are shown in Figs. 19a and b for the same orientations.

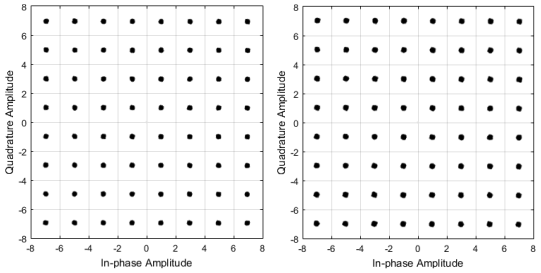

(a) (b)

Fig. 18. Constellation diagram at 3.5 GHz for (a) broadside and (b) second orientation.

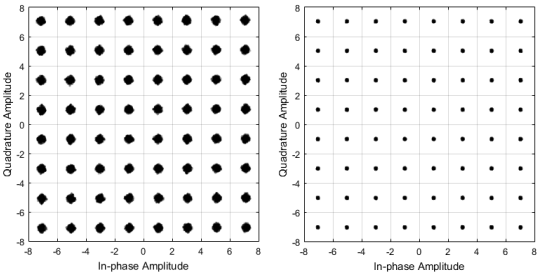

(a) (b)

Fig. 19. Constellation diagram at 6 GHz for (a) broadside and (b) second orientation.

The communication properties as well as the EVM and BER results for the two carrier frequencies at the two orientations are summarized in Table II. The EVM for the digital communication system at 6 GHz was found to be 3.25% and 0.91% for the broadside and second orientation, respectively. The receiver was able to recover the symbols for both carrier frequencies at the two orientations, and the BER was found to be zero. The reason for the symbol scattering in the broadside is the low transmission at 6 GHz caused by the large variation of antenna gain within the frequency range 6 GHz to 8 GHz in this direction. The second orientation was found to have a higher UWB than the broadside. The EVM can be further improved if equalization is applied at the receiver. These simulations thus confirm that the second orientation is preferable for the whole UWB in digital communication systems because of the low symbol scattering at 6 GHz.

Although the antenna itself is wideband—in terms of total radiated power (S_{21}^a)—for P2P communications, the antenna provides different frequency response patterns for different orientations. A system operating at 3.5 GHz showed no difference in EVM values between the two orientations. At 6 GHz, however, the second orientation performs better than the broadside orientation, where symbol scattering can be observed. The P2P communication thus primarily depends not only on the bandwidth or the carrier frequency of the system but also on the antenna orientation. This situation enables P2P communication system designers to choose the proper operating frequency according to antenna orientation.

TABLE II
DIGITAL COMMUNICATION SYSTEM PARAMETERS

Antenna orientation	Broadside		Second orientation	
Modulation scheme	64-QAM		64-QAM	
Samples per symbol	1		1	
RF frequency	3.5 GHz	6 GHz	3.5 GHz	6 GHz
EVM	1.40%	3.25%	1.42%	0.91%
BER	0	0	0	0

VI. CONCLUSION

In this study, a process was developed to characterize the frequency response of UWB antennas for P2P communications. The Friis equation was modified in terms of total radiated power and measured radiated power in the physical channel to calculate the effective aperture and gain. This process will provide antenna designers with useful insights into the variation of radiation patterns across the frequency band in certain directions. The frequency response of the non-minimum phase UWB antenna was also investigated in two orientations.

A frequency-dependent equivalent circuit was derived from only measuring S_{11} in amplitude and phase. The total radiated power calculated from the equivalent circuit was shown to provide the radiated power in all directions from the antenna. In addition, designers can use the phase of S_{21}^{a} obtained from the equivalent circuit to determine the predicted behavior of the antenna over the frequency band.

The phase of S_{21} for each orientation was separated into three components: linear, minimum, and all-pass phases. Having an all-pass component means that there is resonant structure in the frequency band, resulting in a variant radiation pattern with respect to the frequency. A minimum phase antenna will have a frequency-invariant radiation pattern and non-resonant structure over the band on its principal axis. Constant gain means that the GD of S_{21} is constant and that there is no all-pass component. The frequency response in terms of the effective aperture, gain, phase of S_{21}, and GD confirmed that the antenna performance was acceptable for P2P communications in the second orientation, where the azimuth and elevation angles were 90° and 45°, respectively. The effects of the antenna on digital modulation were also observed for the two orientations, which demonstrated that the effects of the antenna in the second orientation were acceptable compared to the broadside. Future work will include a multipath-rich environment in P2P communications and a study of the performance and behavior of the antenna as well as the S_{21} transmission phase.

REFERENCES

[1] D. Panaitopol et al., "Impact of the design of an UWB antenna on the maximum achievable rate of the communication in presence of multi user interferences," in *Asia-Pacific Micro. Conf.*, 2008.

[2] G. S. Reddy, S. Kharche, and J. Mukherjee, "Ultra wideband printed monopole antenna with curve shaped extended asymmetric CPW ground plane for stable unidirectional radiation pattern," in *IEEE Ant. Prop. Soc. Int. Symp. (APSURSI)*, 2014.

[3] F. Fereidoony, S. Chamaani, and S. A. Mirtaheri, "Systematic design of UWB monopole antennas with stable omnidirectional radiation pattern," *IEEE Ant. Wire. Prop. Lett.*, vol. 11, pp. 752-755, 2012.

[4] S. K. Ghosh and R. K. Badhai, "Printed monopole antenna for UWB and SWB with directional radiation characteristics and high F/B ratio," in *Int. Conf. Wire. Comm., Sig. Proc. and Netw. (WiSPNET)*, 2016.

[5] T. Dissanayake and K. P. Esselle, "UWB performance of compact L-shaped wide slot antennas," *IEEE Trans. Antenna Prop.*, vol. 56, no. 4, pp. 1183-1187, 2008.

[6] O. K. Heong, C. K. Chakrabarty, and G. C. Hock, "Circuit modeling for rectangular printed disc monopole antenna with slot for UWB system," in *Third Int. Conf. Intell. Syst. Mod. and Sim.*, 2012.

[7] Y. Wang, T. Jiang, and Y. Li, "Equivalent circuit model of a triple frequency rejection band UWB antenna," in *Int. App. Comp. Electromag. Soc. Symp.*, Italy (ACES), 2017.

[8] S. J. Wu et al., "Study of an ultrawideband monopole antenna with a band-notched open-looped resonator," *IEEE Trans. Antenna Prop.*, vol. 58, no. 6, pp. 1890-1897, 2010.

[9] J. S. McLean, R. Sutton, and H. Foltz, "Minimum phase/all-pass decomposition of LPDA transfer functions," in *IEEE Int. Conf. Ultra-Wideband*, 2009.

[10] H. Foltz et al., "UWB antenna transfer functions using minimum phase functions," in *IEEE Ant. Prop. Soc. Int. Symp.*, 2007.

[11] J. S. McLean, H. Foltz, and R. Sutton, "Differential time delay patterns for UWB antennas," in *IEEE Int. Conf. Ultra-Wideband*, 2008.

[12] J. S. McLean, H. Foltz, and R. Sutton, "Directional dependence of the minimum phase property of antenna transfer functions," in *Ant. & Prop. Conf. LAPC 2009*. Loughborough, UK, 2009.

[13] H. D. Foltz et al., "Non-minimum phase behavior due to fractional Hilbert transform in broadband circular polarization antennas," in *Electromagnetic Theory (EMTS), URSI Int. Symp. on*, 2010.

[14] P. Bahramzy and G. F. Pedersen, "Group delay of high Q antennas," in *IEEE Ant. Prop. Soc. Int. Symp. (APSURSI)*, IEEE, 2013.

[15] M. I. Sobhy, B. Sanz-Izquierdo, and J. C. Batchelor, "System and circuit models for microwave antennas," *IEEE Trans. on Micro. Theory and Tech.*, vol. 55, no. 4, pp. 729-735, 2007.

[16] C. A. Balanis, "Antenna vector effective length and equivalent areas," in *Antenna Theory*, 3rd ed. New Delhi: Beekam Print & Pack, 2015, pp. 89-96.

[17] D. M. Pozar, "The scattering matrix in microwave network analyzer," in *Microwave Engineering*, 4th ed. New Jersey: John Wiley & Sons, 2012, pp. 177-183.

[18] H. Aumann, T. Schmitt, and D. Mooradd, "A modification of the two-antenna method to determine the phase center location as well as the gain of a wideband antenna," in *IEEE Int. Symp. on Ant. Prop. & USNC/URSI Nat. Radio Sci. Meeting*, 2015.

[19] H. Y. Lam, "Properties of network functions," in *Analog and Digital Filters: Design and Realization*, L. O. Chua, ed. Upper Saddle River, NJ: Prentice-Hall, 1979, pp. 55-61.

[20] H. Schantz, "A taxonomy of UWB antennas," in *The Art and Science of Ultrawideband Antennas*, London: Artech House, 2005, pp. 214-227.

Mohammed A. Almoteriy received the B.sc. and M.Sc in electronics and communications engineering from the University of King Abdulaziz, Jeddah, KSA in 1998 and 2005, respectively.
He is currently pursuing the Ph.D. degree with the Communication Research Group at the University of Kent. His current research interests include Antenna and Channel Modeling for Indoor Applications.

Mohamed I. Sobhy received the B.Sc. degree in electrical engineering from the University of Cairo, Cairo, Egypt, in 1956, and the Ph.D. degree from the University of Leeds, UK, in 1966.
Currently, he is an Emeritus Professor of Electronics with the University of Kent, Canterbury, U.K. His research interest include analysis and applications of nonlinear electronic systems.

John C. Batchelor (S'93–M'95–SM'07) received the B.Sc. and Ph.D. degrees from the University of Kent, Canterbury, U.K., in 1991 and 1995, respectively.
He was a Research Assistant with the Electronics Department, University of Kent, from 1994 to 1996, where he became a Lecturer of electronic engineering in 1997. He currently leads the Antennas Group, University of Kent, where he is also a Professor of antenna technology. His current research interests include ultra-high frequency radio frequency identification tag design, passive sensing, body-centric antennas, printed antennas, compact multiband antennas, electromagnetic bandgap structures, and long wavelength frequency-selective surfaces.